J Mater Sci (2011) 46:6627–6632
DOI 10.1007/s10853-011-5613-6

Growth of Al_2O_3 thin film by oxidation of resistively evaporated Al on top of SnO_2, and electrical properties of the heterojunction SnO_2/Al_2O_3

Jorge L. B. Maciel Jr. · Emerson A. Floriano · Luis V. A. Scalvi · Leandro P. Ravaro

Received: 22 October 2010 / Accepted: 7 May 2011 / Published online: 19 May 2011
© Springer Science+Business Media, LLC 2011

Abstract Aiming for the investigation of insulating properties of aluminum oxide (Al_2O_3) layers, as well as the combination of this oxide with tin dioxide (SnO_2) for application in transparent field effect transistors, Al thin films are deposited by resistive evaporation on top of SnO_2 thin films deposited by sol–gel dip-coating process. The oxidation of Al films to Al_2O_3 are carried out by thermal annealing at 500 °C in room conditions or oxygen atmosphere. X-ray diffraction data indicate that tetragonal Al_2O_3 is indeed obtained. A simple device and electric circuit is proposed to measure the insulating properties of aluminum oxide and the transport properties of SnO_2 as well. Results indicate a fair insulation when four layers or Al_2O_3 are grown on the tin dioxide film, concomitant with thermal annealing between each layer. The current magnitude through the insulating layer is only 0.2% of the current through the semiconductor film, even though the conductivity of the SnO_2 alone is not very high (the average resistivity is 2 Ω cm), because no doping is used. The presented results are a good indication that this combination may be useful for transparent devices.

Introduction

The seeking for materials with desired dielectric properties for application in logical electronics has attracted a great deal of attention and research, particularly deposition of aluminum oxide (Al_2O_3) layers on devices based on gate dielectric [1, 2]. Al_2O_3 is among the very interesting materials for this role due to some peculiar properties, such as high dielectric constant ($\varepsilon/\varepsilon_o$ about 8.6 to 10), low leakage current, high thermal stability and high optical bandgap ($\sim$9 eV) [3], deserving a deep investigation. These properties make this oxide very competitive to the widely used silicon dioxide (SiO_2) which has been used as insulating layer in field effect transistor metal–oxide–semiconductor (MOSFET) [4, 5]. By applying a voltage in the gate of the transistor, the electronic transference between source and drain [6] may be efficiently controlled if the oxide used in the gate presents high dielectric constant [7] and low leakage current. High-*k* dielectrics Al_2O_3, also known as alumina, has been successfully used for this role [2, 5].

Although many techniques have been proposed to deposition of alumina thin films [3, 5, 8–10], in this work a rather simpler technique is used: resistive evaporation of aluminum (Al) followed by oxidation in appropriate atmosphere, to Al_2O_3. In this technique, the aluminum metal is heated until evaporation, being deposited on a substrate as a thin film. Considering that alumina has a relatively high boiling temperature, 2980 °C [11], the deposition of alumina directly on the substrate would be hard. Aluminum has a slightly lower evaporation point, in normal condition 2519 °C [12], besides this temperature decreases drastically with the decrease of vapor pressure [13]. Considering the low pressure used in the evaporation chamber, the deposition of Al is rather convenient.

On the other hand, tin dioxide (SnO_2) is a wide-bandgap semiconductor (3.6–4.0 eV [14]), with fair chemical stability and very useful optical and electrical properties [15]. It has been widely used in several types of devices, such as gas sensors [16, 17], transparent conducting electrodes [18],

J. L. B. Maciel Jr. · E. A. Floriano · L. P. Ravaro
Programa de Pós Graduação em Ciência e Tecnologia de Materiais, FC, State University of São Paulo (UNESP), 17033-360 Bauru, SP, Brazil

L. V. A. Scalvi (✉)
Physics Department, FC, State University of São Paulo (UNESP), 17033-360 Bauru, SP, Brazil
e-mail: scalvi@fc.unesp.br

and optoelectronic devices [19]. It presents high transparency in the visible and is a good matrix for doping with luminescent ions such as rare earths [20, 21]. Combination of SnO_2 with other materials, constituting heterojunctions, is not a novelty. However, the combination proposed here (SnO_2/Al_2O_3) may be useful towards the fabrication of transparent MOSFETS. SnO_2 has also been combined with gallium selenide (GaSe), a wide-bandgap semiconductor, becoming also a prospective combination for use in optoelectronic devices. SnO_2/GaSe heterojunctions, having optically transparent SnO_2 electrodes, have been deposited by thermal oxidation or by magnetron sputtering [22]. Surface states where charge carrier recombination can occur are formed at the interface during deposition of the SnO_2 layer. The presence of a high concentration of defects determines the structure of the PL spectrum [22]. Most recently a combination of SnO_2 and GaAs grown by the same techniques proposed here (sol–gel dip-coating and resistive evaporation, respectively) [23] led to very interesting electrical behavior of the heterojunction, concerning the interface between the GaAs film and the SnO_2 film, which exhibited good quality and lower resistivity when compared with the individual films.

Aiming for the combination of a transparent oxide semiconductor (with technologically desirable properties), along with an insulating oxide, which is also transparent in the form of thin film, the deposition of Al on top of a SnO_2 thin film was performed in this work, generating a simple SnO_2/ Al_2O_3 heterostructure after thermal annealing. It is expected that the thin films deposited by both of these processes will naturally contain a high density of structural and interfacial defects. However, the electrical characteristics of the resulting heterojunction, evaluated through current–voltage data for several temperatures, point to very promising performance, related to the low leakage current through the alumina layer, when an appropriate number of layers is grown.

Experimental

The preparation of the alcoholic SnO_2 solution has $SnCl_4{\cdot}5H_2O$ as precursor and ethylic alcohol (C_2H_6O) as solvent [24], which was dissolved under stirring with a magnetic bar, followed by addition of NH_4OH until pH reaches 11. Ions Cl^- and NH^{4+} were eliminated by dialysis against distilled water. Films were deposited on silicate glass substrates by dip-coating with 10 cm/min dipping rate. Multi-dipped films were continuously deposited at room temperature with firing at 400 °C for 10 min after each dip. Resulting SnO_2 film (10 layers) was thermally annealed (T.A.) at 550 °C for 1 h.

Al evaporation was done by the resistive evaporation technique, with 10^{-5} mbar of pressure in an EDWARDS Auto 500 evaporation system, with tungsten filaments to provide the Al wire heating. The metal was deposited on the top of the SnO_2 layer. Several aluminum layers were deposited and after each layer the sample was submitted to thermal annealing at 500 °C for 1 h in air atmosphere. Sn electrodes have also been evaporated through the same technique and system, to make electric contacts to the films, in order to accomplish electrical measurements, using Sn shots placed on a molybdenum crucible. Sn electrodes were submitted to thermal annealing at 150 °C for 30 min.

X-ray diffraction (XRD) data on films were obtained with a RIGAKU diffractometer, model D/MAX-2100/PC, using Cu K_α radiation (1.5406 Å) and a Ni filter for elimination of K_β radiation. The scanning rate was 1°/min in the range 20° to 80°.

Current as function of temperature measurements were carried out under vacuum conditions, in a closed helium circuit cryostat of Janis Research, coupled with a Lake Shore Cryotronics temperature controller with 0.05° of precision. The experimental setup is seen in Fig. 1a. The source–drain current were measured with a Agilent Multimeter model 34401A, whereas the source–gate (leak current) were measured with a Keithley Electrometer model 6517A. The lateral view of the resulting sample is shown in Fig. 1b.

Results and discussion

Figure 2 presents X-ray diffractograms for films with six Al layers deposited on borosilicate substrates, followed by thermal annealing (T.A.) between each layer in different

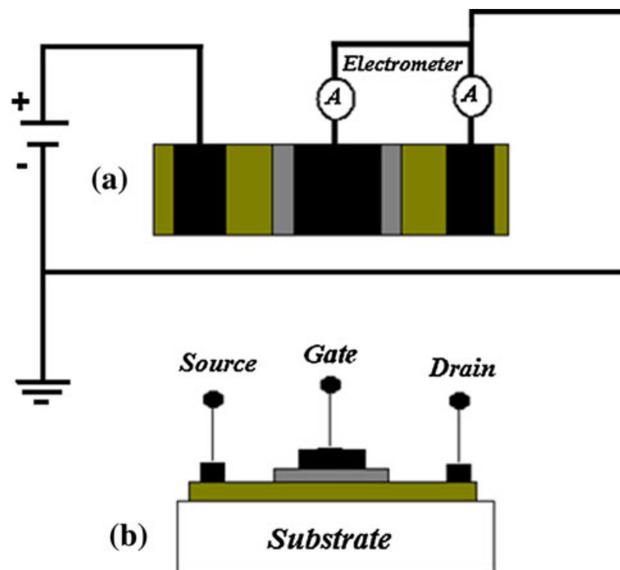

Fig. 1 Diagram of the device used for electrical characterization. **a** Top view showing the electrical connections and **b** cross-section view, using alumina as gate and Sn contacts (electrodes)

atmospheres (oxygen or air). The labeled peaks correspond to the CRYSTMET ID-477212 pattern, tetragonal alumina. Table 1 shows the experimental diffraction angles corresponding to curves (i) and (ii) of Fig. 2, compared to the standard X-ray file (CRYSTMET ID-477212). Tetragonal alumina has been observed for materials thermally annealed between 500 and 700 °C [25] in good agreement with our results, and the tetragonal character of the alumina decreases for annealing temperatures above 700 °C. Many other alumina phases have been identified for annealing temperatures in the range 900–1100 °C [26]. Table 2 shows the crystallite size for the main identified alumina directions evaluated according to the Scherrer equation [27]. Previous to any thermal annealing, the Al X-ray diffractogram (not shown) indicates FCC Aluminum structure (CRYSTMET card number ID 35673). In Fig. 2, the experimental Al peaks were subtracted from the diffractograms pattern.

It is easily verified from Table 1, that the major difference ($|\Delta\theta|$) between experimental values (obtained from Fig. 2) and crystallographic reference values (CRYSTMET card number ID 477212), in the experimental range 20° to 80°, was 0.7 at 36.7°. The most intense peaks of the reference in the investigated range (20°–80°) are associated to plans (0012), (220), (2212) and (400), located at 44.5°, 45.7°, 65.7°, and 66.6°, respectively, in very good agreement with the observation shown in Fig. 2, for both difractograms, as also described in Table 1. Previous to the subtraction of Al peaks from Fig. 2, there are Al peaks at 38.5° and 78.2°, corresponding to (111) and (311) plans of FCC Aluminum (CRYSTMET card number ID 35673). These values are also observed in the experimental

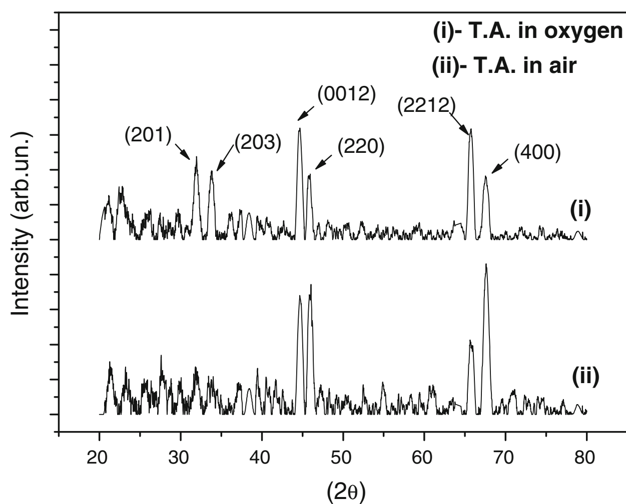

Fig. 2 X-ray diffractograms of alumina films obtained from Al oxidation, thermally annealed (T.A.) in different atmospheres (air or oxygen-rich). Al peaks of the diffractogram of the starting material were subtracted

diffractogram (not shown) of as-deposited Al films, previously to any T.A. Then, considering the deposition process procedure, the presence of these peaks is probably related to the remaining non-oxidized Al in the annealed film, indicating that the oxidation process may not be completely homogeneous throughout the film surface. Figure 2 also allows inferring that the distinct atmosphere (oxygen or air) does not lead to significant differences in the Al_2O_3 film structure. There is also no meaningful difference between the average crystallite size (Table 2) of these two annealing procedures. The estimated sizes are in good agreement with the broaden profile of the peaks, characteristic of nanocrystallites domains. The oxygen atmosphere only contributes to a better definition of the diffractogram pattern when compared to the simpler air atmosphere. Although the oxidation is not complete all over the film surface, the X-ray diffractograms shown in Fig. 2 assures that the oxidation procedure leads to tetragonal alumina. Figure 3 shows a scanning electron microscopy (SEM) picture of the film surface, which was thermally annealed in oxygen atmosphere. It is easily seen that there are some heterogeneities in the surface, consequence of the deposition procedure itself.

Infrared spectroscopy (not shown) presented a sharp peak about 560 cm^{-1}, which may be associated with Al–O vibration [28]. Investigation on the annealing time at 500 °C reveals the increase in the films transparency with time, suggesting that oxidation of Al to Al_2O_3 is a slow reaction. The diffractogram of these films show that the presence of alumina with tetragonal structure is independent of film thickness and becomes noticeable for about 60 min of thermal annealing at 500 °C, which is exactly the annealing time used in this work.

Electrical characterization through current–voltage ($I \times V$) measurements are carried out for several temperatures, and the results are shown in Fig. 4, using the device with four alumina layers on the gate (about 200 nm of thickness). The characterization of a heterojunction sample of SnO_2/Al_2O_3 with only one layer of alumina (about 70 nm) in the gate, leads to similar magnitudes of source–drain and source–gate currents. However, when the number of layers is increased to 4, leading to a thickness of about 200 nm, the magnitude of the current is of 6.54×10^{-8} A for the source–gate and 30.7×10^{-6} A for the source–drain, considering an applied voltage of 40 V, which means that only 0.2% of the current is lost through the gate as leakage current. The importance of this result is significantly intensified by taken into account that the SnO_2 film is undoped and the conductivity is not high ($\sigma = 0.5$ S cm^{-1}). The conductivity can be significantly increased by a doping procedure with Sb [29] or F [30], for instance. It is expected that the deposition of Al layer along with the T.A. procedure at 500 °C for oxidation to Al_2O_3

Table 1 Comparison between diffractograms angles obtained for the films produced through T.A. in different atmospheres and reference CRYSTMET ID 477212

(*hkl*)	Experimental 2θ T.A. in oxygen (°)	2θ reference ID 477212 (°)	$\|\Delta\theta\|$ between columns 2 and 3	Experimental 2θ T.A. in air (°)	$\|\Delta\theta\|$ between columns 5 and 3
104	21.2	21.5	0.3	21.2	0.3
110	22.9	22.4	0.5	22.9	0.5
114	26.2	26.8	0.6	26.2	0.6
201	32.0	32.1	0.1	32.0	0.1
203	33.9	33.8	0.1	–	–
0010	36.0	36.7	0.7	36.0	0.7
213	37.5	37.5	0	37.5	0
206	39.6	39.1	0.5	39.6	0.5
0012	44.7	44.5	0.2	44.7	0.2
220	45.9	45.7	0.2	45.9	0.2
223	47.1	47.1	0	47.1	0
2212	65.2	65.7	0.5	65.2	0.5
400	66.9	66.6	0.3	66.9	0.3

Table 2 Crystallite size estimation on main directions

Al_2O_3 film	Crystallite size (nm)			
	(0012)	(220)	(2212)	(400)
T.A. in O_2	11.6	14.0	12.7	12.1
T.A. in air	12.6	12.6	12.7	12.6

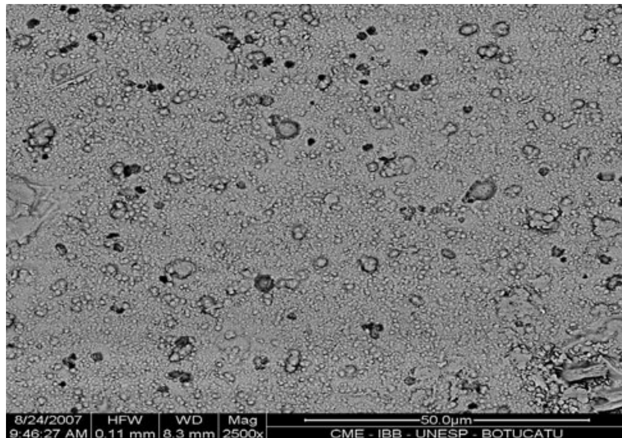

Fig. 3 Scanning electron microscopy (SEM) of Al_2O_3 sample surface of a film with six layers

must lead to an heterogeneous surface, where the presence of porous (holes) through the treated materials is not surprising. The irregularities on the surface are seen in Fig. 3, where a SEM picture of the surface of a sample with six alumina layers is shown. Besides, the oxidation is not as effective as expected, due to the observation of some FCC Aluminum peaks in the diffractograms. Then, the alumina layer may lead to direct metallic contact between SnO_2 film and the Sn electrode layer. However, the deposition of a series of layers inhibits the percolation of pores, and a better insulation in the gate is obtained. As the temperature decreases, the magnitude of the current in the conduction channel (source–drain) decreases, as expected for a semiconductor and, then, the current through the gate becomes also lower, although presents a relative higher value when compared to the drain current. At 100 K, the source–gate current is still lower than the source–drain current but they present comparable magnitudes. It should be noticed that as the temperature is decreased, the electron capture in the SnO_2 semiconductor channel increased the insulator behavior of this material, and in this case, the current must be divided between the two insulator paths: SnO_2 and Al_2O_3. As the temperature is increased the general growth of the current magnitude in the semiconductor film leads to a relative better insulation in the alumina gate layer.

Figure 5 shows the ratio of current source–gate to source–drain, obtained for several temperatures. It can be observed that, except for the measurement carried out at 250 K, there is general tendency for the ratio to become close to unit as the temperature is decreased. This temperature-dependent behavior of the current ratio gate/drain confirms the electron capture in the semiconductor layer, leading to a resistivity increase in this film and then, comparable insulating paths when the temperature reaches 100 K. At 250 K, this ratio as not as low as expected and a peculiar behavior is observed, where besides the higher current source–gate when compared to source–drain, the $I \times V$ characteristics of the source–drain current is not linear, suggesting that the Sn electrode deposited on the SnO_2 film may be playing a different role in this temperature. It is interesting to mention that the decay of photo-induced conductivity measurements carried out for SnO_2

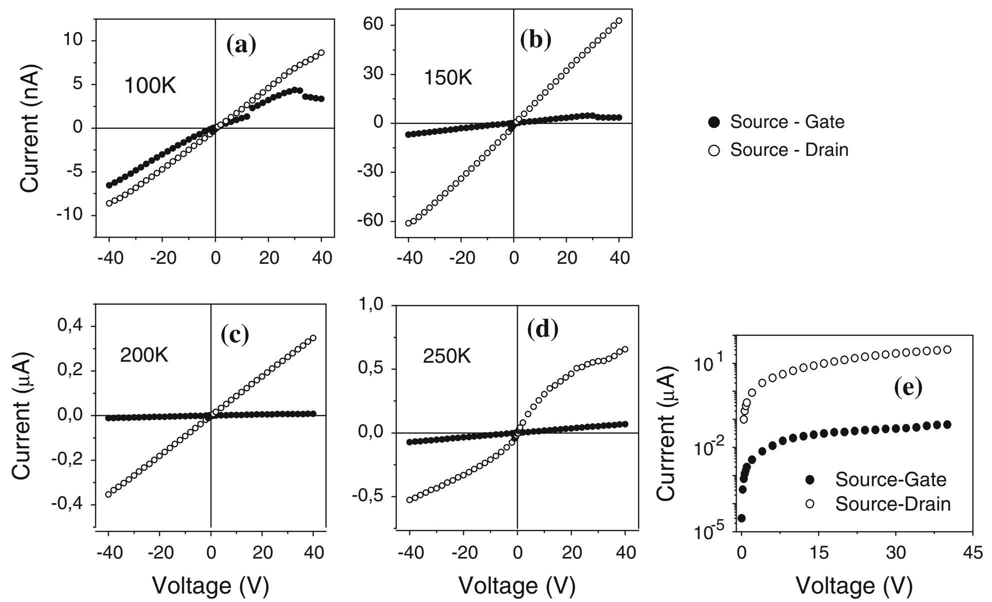

Fig. 4 Current as function of voltage for heterojunction SnO_2/Al_2O_3 at distinct temperatures: 100 K (**a**), 150 K (**b**), 200 K (**c**), 250 K (**d**), and 300 K (**e**)

films [31] reveals that this temperature is in the range where the capture by defects is the most active, including trapping by oxygen vacancies [32]. This information is very relevant for the simple device proposed here, because the sample is not doped, and then, the vacancies are the most efficient donors in the n-type SnO_2 undoped semiconductor. Then, the depletion layer close to the interface metal–semiconductor is influenced by the electron trapping by oxygen vacancies, which does not affect the conduction mechanism when the temperature is further decreased, because the interfacial layer is completely depleted and the overall resistivity is higher, as shown by the results presented in Fig. 4. However, the probable depletion of the interfacial layer is a matter for future investigation.

The alumina layer insulation, which leads to the results shown in Figs. 4 and 5, indicates that this procedure for achievement of Al_2O_3 layer may be used for production of transparent field effect devices. There is a clear indication that an alumina multilayer deposition procedure must lead to a very efficient electrical insulation, with very low leakage current. Besides, the n-type doping of the SnO_2 film may improve the current magnitude through the semiconductor layer, making the device very useful. Moreover, the conducting layer may be doped with rare-earth luminescent centers, leading to very many possibilities, such as electric field-triggered emission.

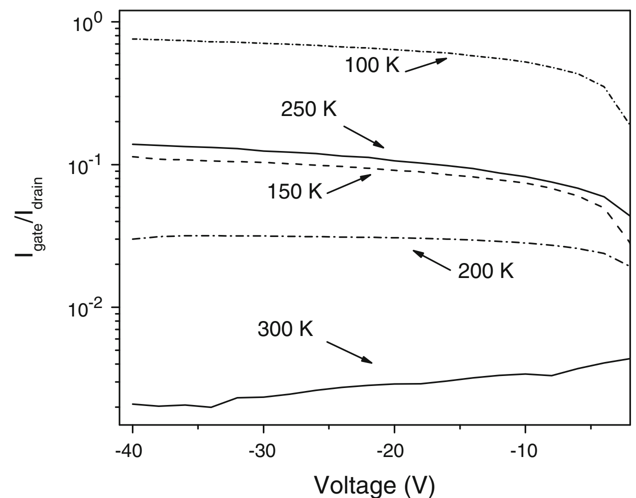

Fig. 5 Ratio of source–gate current to source–drain current, measured at several temperatures

Conclusion

Adding the transparent semiconducting properties of SnO_2 thin films to the insulating properties of Al_2O_3, a potential technologically applicable heterojunction has been created. The simple device assembled here shows that the insulation depends on the number of layers deposited. The possible existence of pores in the single layer has led to a source–gate current comparable to source–drain current, indicating that the contact between SnO_2 and the Sn electrode is independent on the existence of an intermediate alumina layer. However, when the number of alumina layers was increased to four, the insulation increased significantly, suggesting that the deposition of more alumina layers led to much less percolated pores. The electrical characterization of this heterojunction (SnO_2/Al_2O_3) at low temperature (100, 150, 200, and 250 K) presents a gate current lower than the drain current, and the ratio of source–gate current to source–drain current increases with temperature lowering (gets close to the unit), showing the electron trapping in

the SnO_2 layer, characteristic behavior of a semiconductor. Moreover, it shows the potentiality of this array for room temperature applications.

Films obtained through deposition of aluminum and oxidation at 500 °C to Al_2O_3 presents tetragonal alumina structure as shown by X-ray diffraction data, no matter the atmosphere of thermal annealing.

The formation of SnO_2/Al_2O_3 heterojunction, with alumina layer obtained from deposited Al layer with thermal annealing, may be seen as a potential technique for application in transparent transistor production, mainly due to its simplicity.

Acknowledgements Authors would like to thank Brazilian financial sources: CAPES, CNPq, and FAPESP.

References

1. Wu YQ, Xuan Y, Shen T, Ye PD (2007) Appl Phys Lett 91:022108
2. Wu YQ, Ye PD, Wilk GD, Yang B (2006) Mater Sci Eng B 135:282
3. Lin HC, Ye PD, Wilk GD (2006) Solid State Electron 50:1012
4. Srikanth S, Karmalkar S (2008) IEEE Trans Electron Dev 55:3562
5. Xuan Y, Lin HC, Ye PD (2006) Appl Phys Lett 88:263518
6. Crupi I, Degraeve R, Govoreanu B, Brunco DP, Roussel P, Houdt JV (2007) Microeletron Reability 47:525
7. Bhowmick S, Alan K (2008) J Appl Phys 104:124308
8. Ogita Y, Kudoh T, Sakamoto F (2008) Thin Solid Films 516:832
9. Nasution IA, Velesco A, Kim H (2009) J Cryst Growth 311:429
10. Langereis E, Heil SBS, Knoops HCM, Keuning W, Van de Sanden MCM, Kessels WM (2009) J Phys D Appl Phys 42:073001
11. Kang HK (2005) Surf Coat Technol 190:448
12. Lide DR (2003) CRC handbook of chemistry and physics, 84th edn. CRC Press, Boca Raton
13. Hatch JE (ed) (1984) Aluminum properties and physical metallurgy. American Society for Metals, Novelty, OH
14. Yadav JB, Patil RB, Puri RK, Puri V (2007) Mater Sci Eng B 139:69
15. Wang H, Liang J, Fand H, Xi B, Zhang M, Xiong G, Zhu Y, Qian Y (2008) J Solid State Chem 181:122
16. Adamowics B, Izydorczyk W, Izydorczyk J, Klimasek A, Jakubik W, Zywicki J (2008) Vacuum 82:966
17. Kolmakov A, Zhang Y, Cheng G, Moskovits M (2003) Adv Mater 15:997
18. Goebbert C, Aegerter MA, Burgard D, Nass R, Schmidt H (1999) J Mater Chem 9:253
19. Terrier C, Chatelon JP, Roger JA (1997) Thin Solid Films 295:95
20. Morais EA, Ribeiro SJL, Scalvi LVA, Santilli CV, Ruggiero LO, Pulcinelli SH, Messaddeq Y (2002) J Alloys Compd 344:217
21. Morais EA, Scalvi LVA, Tabata A, De Oliveira JBB, Ribeiro SJL (2008) J Mater Sci 43:345. doi:10.1007/s10853-007-1610-1
22. Cuculescu E, Evtodiev I, Caraman M (2009) Thin Solid Films 517:2515
23. Pineiz TF, Scalvi LVA, Saeki MJ, Morais EA (2010) J Electron Mater 39:1170
24. Bagheri-Mohagheghi MM, Shokooh-Saremi M (2004) J Phys D Appl Phys 37:1248
25. Paglia G, Buckley CE, Andrew L, Rohl AL, Hart RD, Winter K, Studer AJ, Hunter BA, Hanna JV (2004) Chem Mater 16:220
26. Levin I, Gemming Th, Brandon DG (1998) Phys Status Solidi A 166:197
27. Cullity BD (1978) Elements of X-ray diffraction, 2nd edn. Addison-Wesley Publishing Company, Reading, MA
28. Socrates G (2006) Infrared and Raman characteristic group frequencies: tables and charts, 3rd edn. Editora LTC, Rio de Janeiro
29. Shanthi E, Dutta V, Banerjee A, Chopra KL (1980) J Appl Phys 51:6243
30. Bhardwaj A, Gupta BK, Raza A, Agnihotri OP (1981) Solar Cells 5:39
31. Morais EA, Scalvi LVA (2007) J Eur Ceram Soc 27:3803
32. Samson S, Fonstad CG (1973) J Appl Phys 44:4618